

Supporting Information For
Carbene-Catalyzed Intramolecular Cyclization to Access
Inherently Chiral Saddle-Shaped Lactones: Achiral Bases
Alternate Product Chirality

Liwen Wei,^{a,+} Yuhang Chen,^{a,+} Qinglong Zhou,^{a,+} Zhikang Wei,^{a,+} Ting Tu,^b Shichao Ren,^b Yonggui Robin Chi,^{b,c*} Xinglong Zhang,^{d,*} and Xing Yang^{a,*}

^a Key Laboratory of Chemical Biology and Traditional Chinese Medicine (Ministry of Educational of China), Key Laboratory of the Assembly and Application of Organic Functional Molecules of Hunan Province, College of Chemistry and Chemical Engineering, Hunan Normal University, Changsha 410081, P. R. China

^b State Key Laboratory of Green Pesticide, Key Laboratory of Green Pesticide and Agricultural Bioengineering, Ministry of Education, Guizhou University, Guiyang 550025, China

^c School of Chemistry, Chemical Engineering, and Biotechnology, Nanyang Technological University, Singapore 637371, Singapore.

^d Department of Chemistry, The Chinese University of Hong Kong, Shatin, New Territories, Hong Kong, P. R. China

xingyang@hunnu.edu.cn; xinglong.zhang@cuhk.edu.hk; robinchi@ntu.edu.sg

Contents

General methods.....	S2
General procedures	S3
Synthetic applications	S4
Determination of the rotational barriers	S8
Computational Studies.....	S14
Characterization data of the catalytic reaction products	S31
X-ray structure of 2q.....	S70
¹H, ¹³C, and ¹⁹F NMR spectra and HPLC charts.....	S71
References.....	S217

Computational Studies

1 Density functional theory (DFT) calculations

Kohn-Sham density functional theory (KS-DFT) calculations were performed with *Gaussian 16* rev. B.01.³ The global hybrid DFT functional M06-2X⁴ with the Karlsruhe-family basis set def2-SVP^{5,6} for all atoms was used for geometry optimization. M06-2X was chosen as it has shown good accuracy in the study of organocatalytic systems.^{7–17} Minima and transition structures on the potential energy surface (PES) were confirmed as such by harmonic frequency analysis, showing respectively zero and one imaginary frequency. For the gas phase-optimized structures, single point (SP) corrections were performed using M06-2X functional and def2-TZVP^{5,6} basis set for all atoms in the implicit SMD continuum solvation model¹⁸ for dichloromethane (DCM) solvent to improve upon the accuracy of the calculated energies.

Gibbs energies were evaluated at the temperature of 0°C, using Grimme's scheme of quasi-RRHO treatment of vibrational entropies,¹⁹ using the GoodVibes code.²⁰ Vibrational entropies of frequencies below 100 cm⁻¹ were obtained according to a free rotor description, using a smooth damping function to interpolate between the two limiting descriptions. The free energies reported in Gaussian from gas-phase optimisation were further corrected using standard concentration of 1 mol/L,^{21–23} which were used in solvation calculations, instead of the gas-phase 1atm used by default in Gaussian program. Unless otherwise stated, the final SMD(DCM)-M06-2X/def2-TZVP//M06-2X/def2-SVP Gibbs energies are used for discussion throughout. *All Gibbs energy values in the text and figures are quoted in kcal mol⁻¹.*

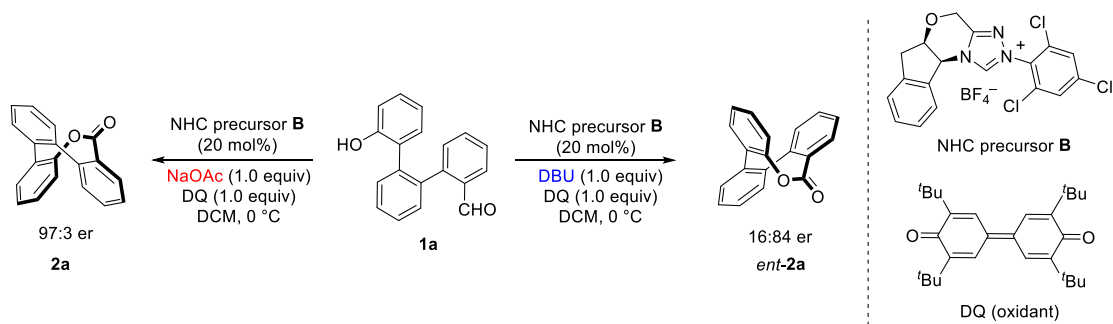
Non-covalent interactions (NCIs) were analyzed using NCIPILOT²² version 4.2 calculations. The .wfn files for NCIPILOT were generated at M06-2X/def2-SVP level of theory. NCI indices calculated with NCIPILOT were visualized at a gradient isosurface value of s = 0.5 au. These are colored according to the sign of the second eigenvalue (λ_2) of the Laplacian of the density ($\nabla^2\rho$) over the range of -0.1 (blue =

attractive) to +0.1 (red = repulsive). Molecular orbitals are visualized using an isosurface value of 0.05 au throughout.

All molecular structures and molecular orbitals were visualized using *PyMOL* software.²⁵

2 Model reaction

Scheme S1 shows the model reactions that were used for computational studies of the reaction mechanism for the NHC-catalyzed base-controlled enantiodivergent synthesis.



Scheme S1. Model reaction used in computational modelling.

3 Conformational considerations

Conformational sampling for key structures was performed using Grimme's *CREST* program,^{26,27} which used metadynamics (MTD) with genetic z-matrix crossing (GC) performed at the GFN2-xTB^{28–30} extended semiempirical tight-binding level of theory with *opt=vtight* option. For the acyl azonium intermediate, the lowest 20 GFN2-xTB energy structures were used for further DFT optimization. The lowest DFT energy structure of the acyl azonium intermediate was used to locate the TS for each base-catalyzed ring closure step. Once the TS was isolated, further constrained conformational sampling of the TS structure fixing the key bond distances was carried out and the lowest 5 GFN2-xTB energy structures were further used as guess structures for TS search using DFT methods. The lowest energy conformer for each pathway was then used for discussion.

4 Acyl azonium intermediate

After conformational sampling and DFT optimization of 20 lowest xTB structures, we identified the lowest energy conformers where the hydroxyl oxygen atom is close to the carbonyl carbon of the acyl azonium, either on the *Re*- or the *Si*- face of the carbonyl C=O group. Structures where these two groups are far way are excluded. The lowest DFT energy conformer for each case (**INT1** and **INT1'**) is shown in Figure S1. Note that **INT1** and **INT1'** are conformers of each other (they result from the conformational sampling of the same structure).

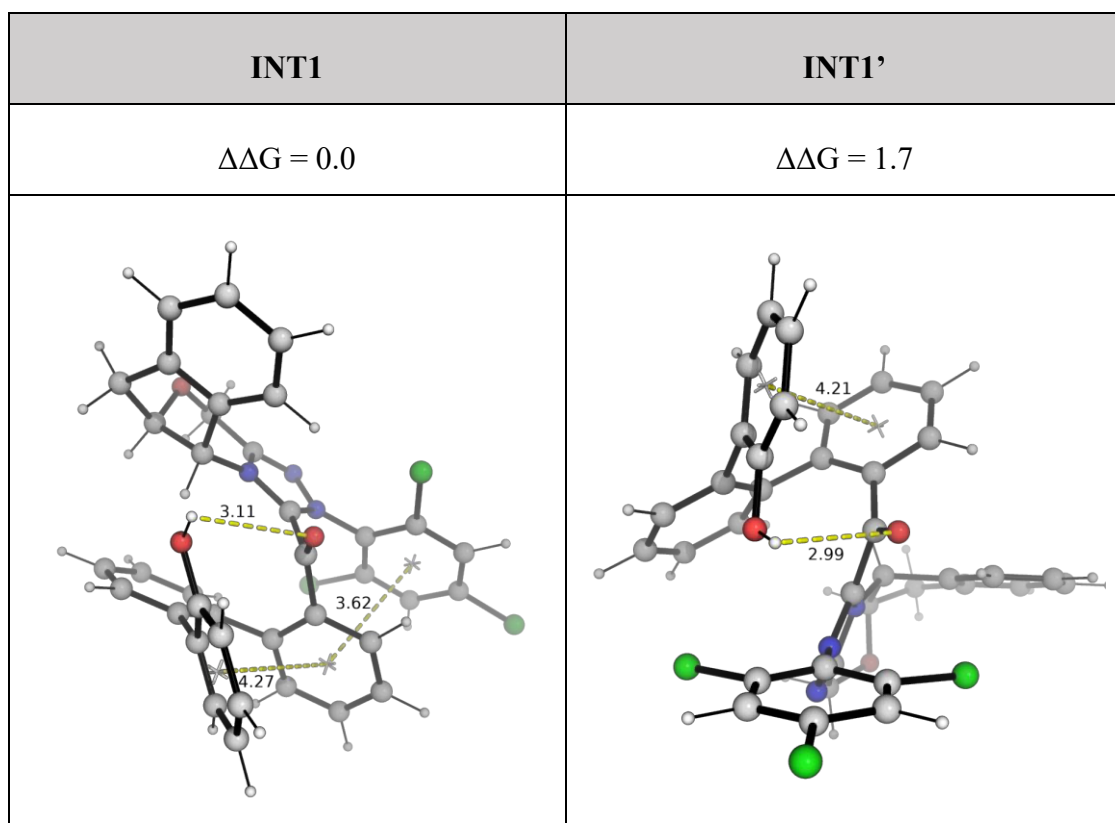


Figure S1. DFT-optimized structures for the lowest energy structure leading to **2a** and *ent*-**2a** via **INT1** and **INT1'** respectively.

5 Enantioselectivity with sodium acetate base

The DFT optimized transition state (TS) structures for the ring closure under sodium acetate base to yield the major (**2a**) and minor (*ent*-**2a**) products are shown in Figure S2. We note that even using 5 lowest xTB energy structures as initial guess for TS

search, some TSs converge to the same structure upon DFT optimization. Relative Gibbs activation barriers, $\Delta\Delta G^\ddagger$, are taken with respect to the TS with the lowest barrier, **TS_NaOAc_major**.

Comparing the lowest barrier transition state (TS) structures leading to the major (**2a**) and minor (*ent*-**2a**) products, we see that the TS leading to the major product, **TS_NaOAc_major**, is lower than the TS leading to the minor product, **TS_NaOAc_minor**, by 1.2 kcal/mol. This translates to an er ratio of 90 : 10 using simple transition state theory (Section 9), in reasonably good agreement with the experimentally observed er ratio of 97 : 3. The analysis of frontier molecular orbitals (HOMO and LUMO) and non-covalent interaction (NCI) plots (Figure S3) suggests that the FMOs are similar for both cases and that **TS_NaOAc_major** may benefit from more favourable non-covalent interactions, making the barrier lower than **TS_NaOAc_minor**.

TS_NaOAc_major	TS_NaOAc_major_c2
$\Delta\Delta G^\ddagger = 0.0$	$\Delta\Delta G^\ddagger = 2.2$
TS_NaOAc_minor	TS_NaOAc_minor_c2
$\Delta\Delta G^\ddagger = 1.2$	$\Delta\Delta G^\ddagger = 3.6$

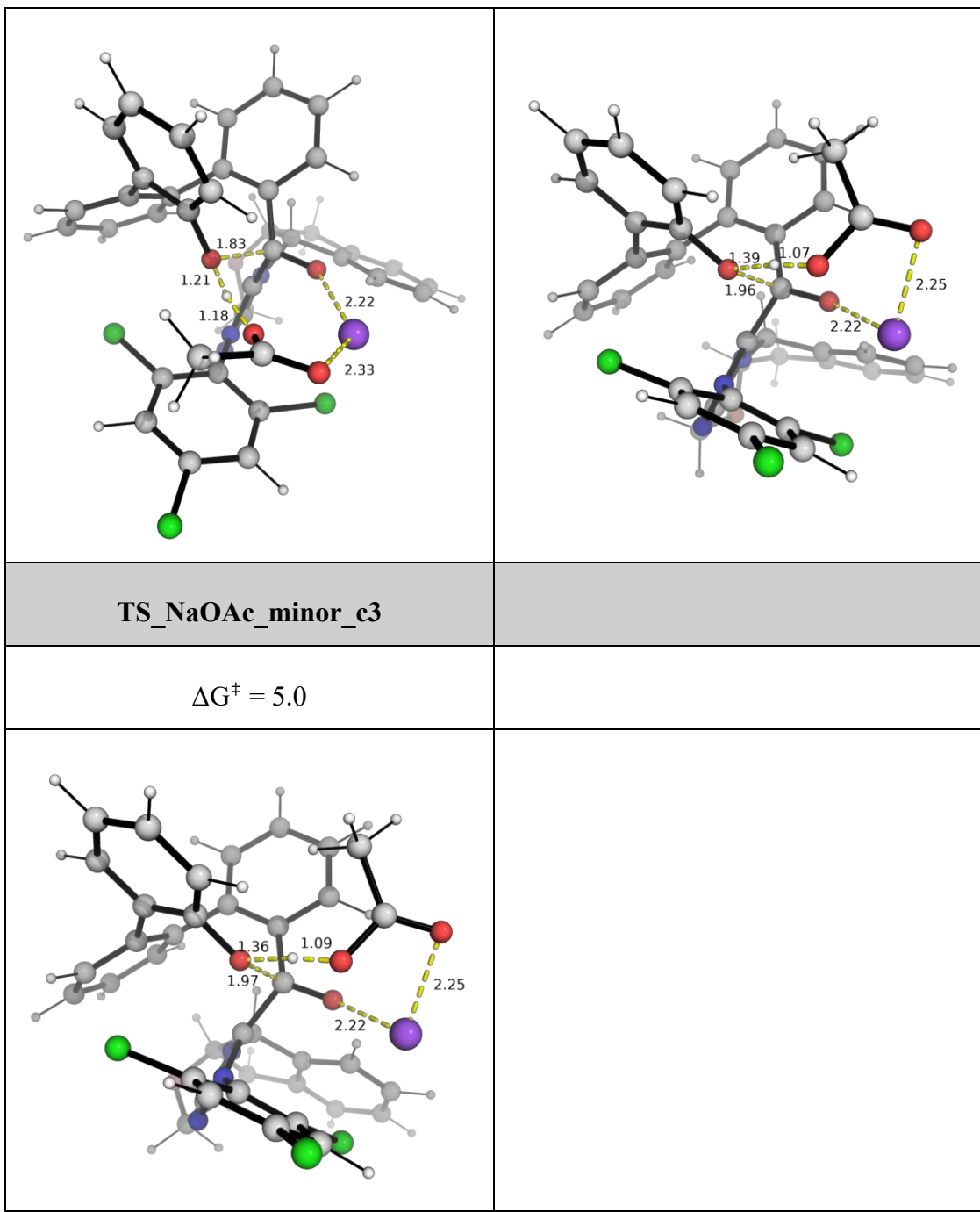
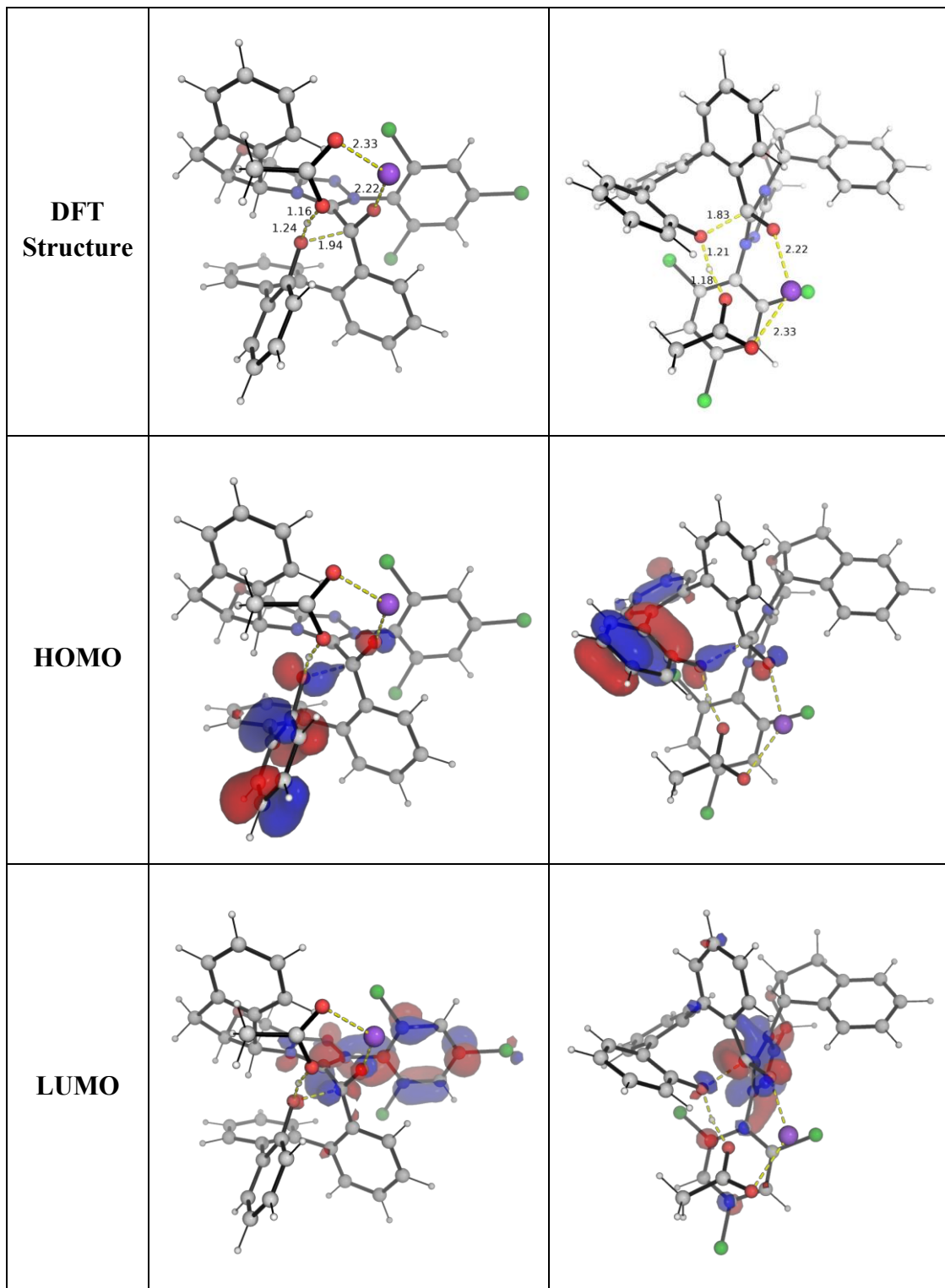


Figure S2. DFT-optimized structures for the transition states for the NaOAc-catalyzed ring closure step for the major and minor pathways leading to major (**2a**) and minor (*ent*-**2a**) products. Relative Gibbs energies are given to the most stable transition state conformer.

	TS_NaOAc_major	TS_NaOAc_minor
barrier	$\Delta\Delta G^\ddagger = 0.0$	$\Delta\Delta G^\ddagger = 1.2$



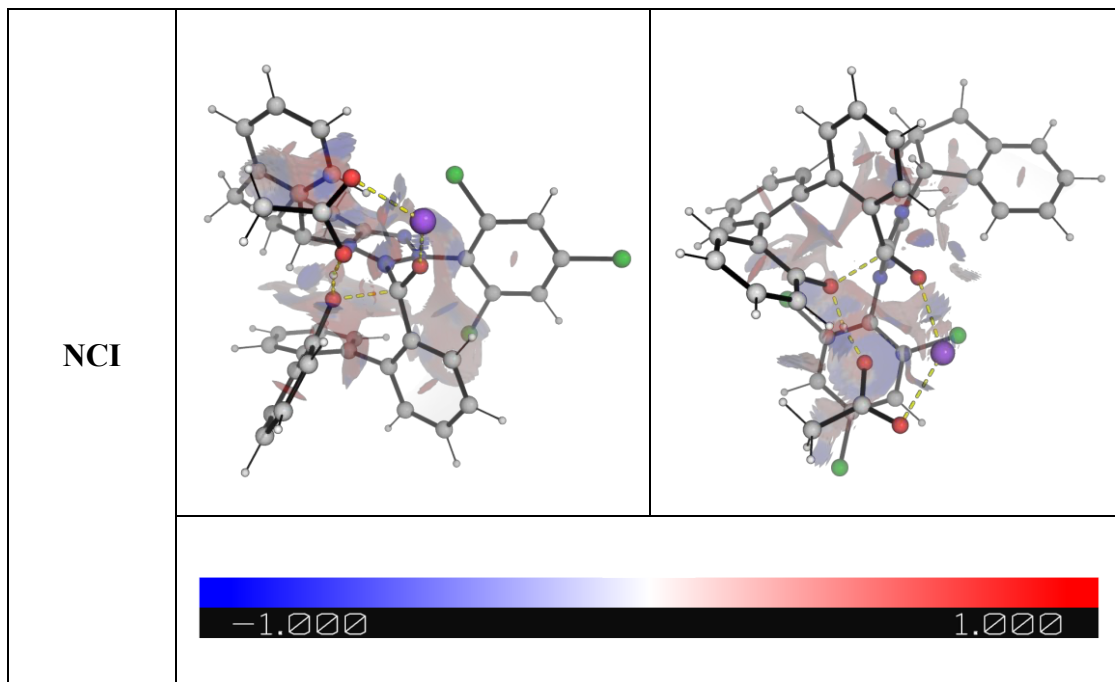
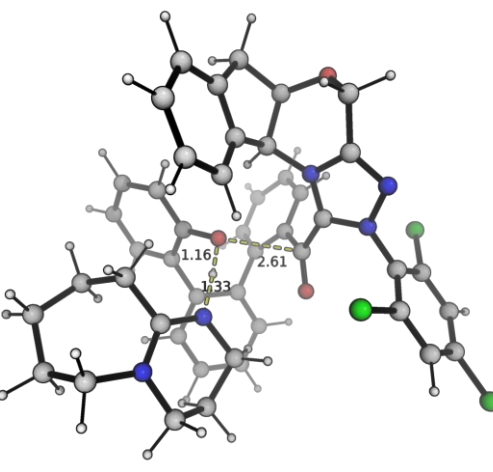
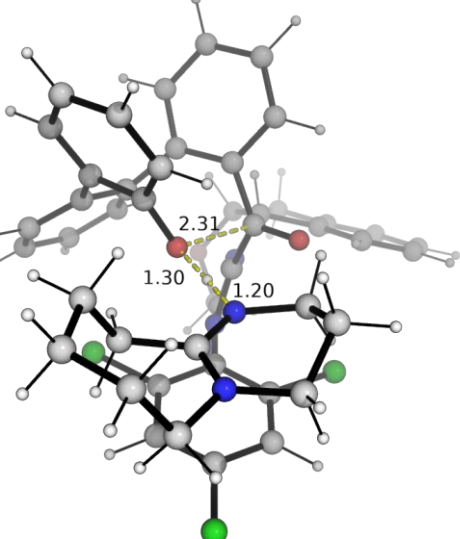
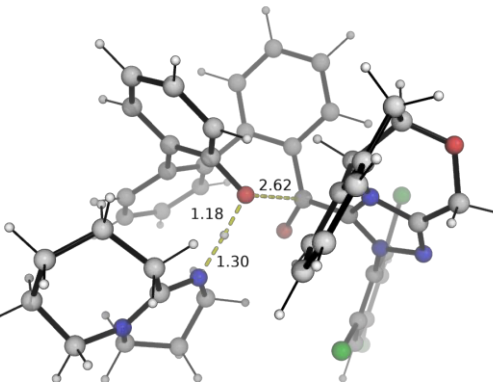
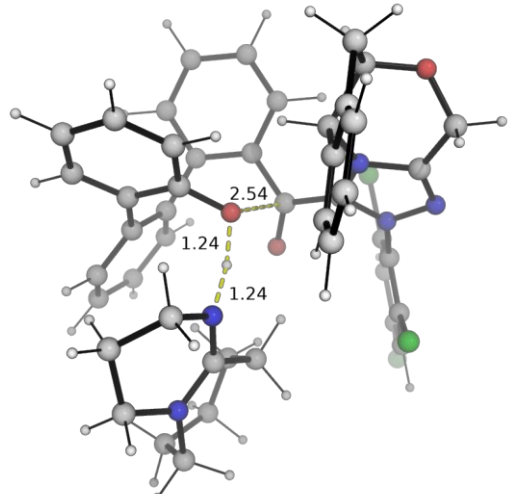


Figure S3. DFT-optimized structures, frontier molecular orbitals (HOMO and LUMO) and non-covalent interaction (NCI) plots for the lowest barrier transition state for the NaOAc-catalyzed ring closure step for the major and minor pathways leading to major (**2a**) and minor (*ent*-**2a**) products.

6 Enantioselectivity with 1,8-Diazabicyclo(5.4.0)undec-7-ene (DBU) base

The DFT optimized transition state (TS) structures for the ring closure under DBU base to yield the major (*ent*-**2a**) and minor (**2a**) products are shown in Figure S5. Relative Gibbs activation barriers, $\Delta\Delta G^\ddagger$, are taken with respect to the TS with the lowest barrier, **TS_DBU_major**.

Comparing the lowest barrier transition state (TS) structures leading to the major (*ent*-**2a**) and minor (**2a**) products, we see that the TS leading to the major product, **TS_DBU_major**, is lower than the TS leading to the minor product, **TS_DBU_minor**, by 0.8 kcal/mol. This translates to an er ratio of 81 : 19 using simple transition state theory (Section 9), in good agreement with the experimentally observed er ratio of 84 : 16. The analysis of frontier molecular orbitals (HOMO and LUMO) and non-covalent interaction (NCI) plots (Figure S5) suggests that the FMOs are similar for both cases. The NCI plots shows that **TS_DBU_major** has more favourable non-covalent interactions than **TS_DBU_minor**.

TS_DBU_major	TS_DBU_major_c2
$\Delta\Delta G^\ddagger = 0.0$	$\Delta G^\ddagger = 0.7$
	
TS_DBU_major_c3	TS_DBU_major_c4
$\Delta\Delta G^\ddagger = 1.1$	$\Delta G^\ddagger = 3.0$
	
TS_DBU_minor	TS_DBU_minor_c2
$\Delta\Delta G^\ddagger = 0.8$	$\Delta\Delta G^\ddagger = 12.8$

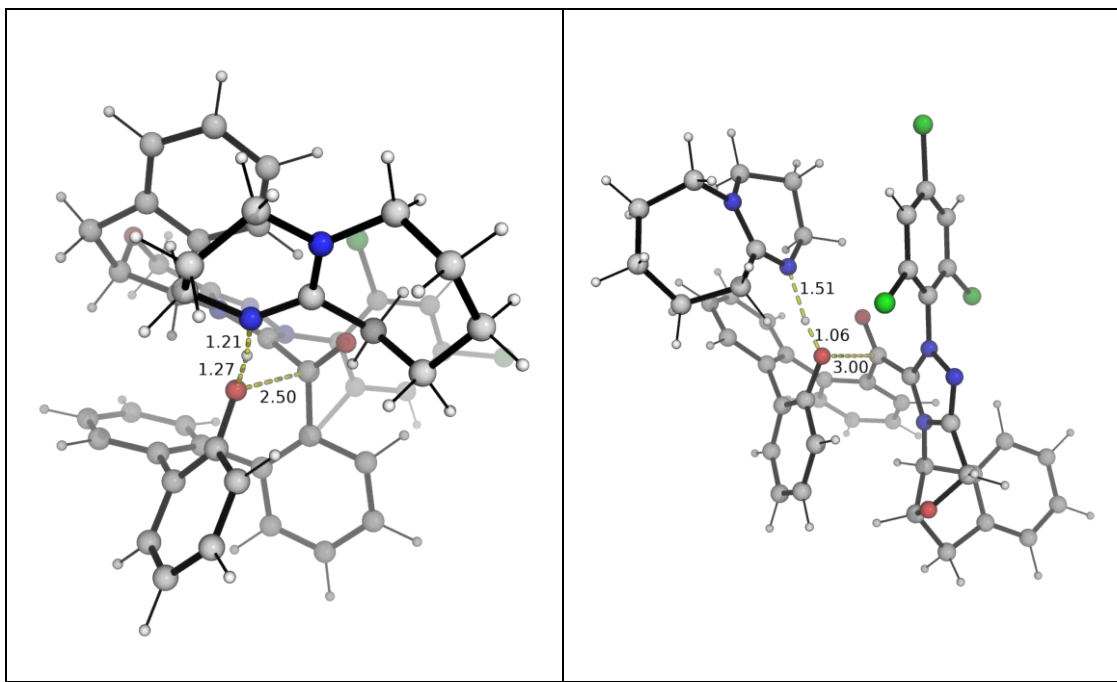


Figure S4. DFT-optimized structures for the transition states for the DBU-catalyzed ring closure step for the major and minor pathways leading to major (*ent*-**2a**) and minor (**2a**) products.

	TS_DBU_major	TS_DBU_minor
barrier	$\Delta\Delta G^\ddagger = 0.0$	$\Delta\Delta G^\ddagger = 0.8$
DFT Structure		

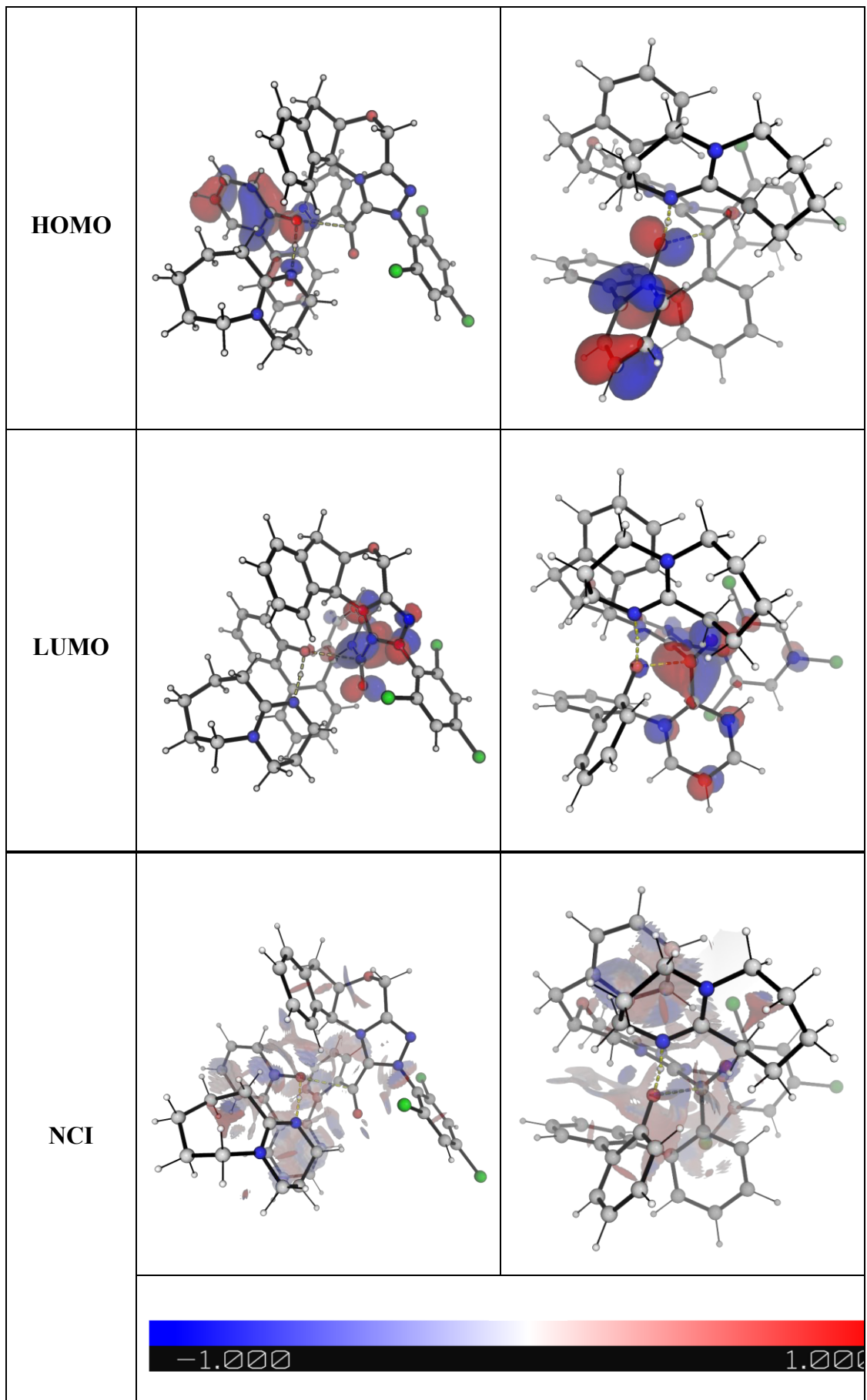


Figure S5. DFT-optimized structures, frontier molecular orbitals (HOMO and LUMO) and non-covalent interaction (NCI) plots for the lowest barrier transition state for the DBU-catalyzed ring closure step for the major and minor pathways leading to major (**2a**) and minor (*ent*-**2a**) products.

7 Distortion-interaction Analysis for enantiodetermining TSs

Distortion-interaction^{31,32} analysis is applied to key TSs to discern the factors affecting enantioselectivity. The transition state structures are decomposed by dividing the base and the acyl azonium intermediate as components. Single point calculations with SMD(DCM) solvent correction were applied performed at M06-2x/def2-TZVP level of theory to obtain distortion and interaction energies. The distortion energy is given by:

$$E_{dist} = E_{TS,frag1} + E_{TS,frag2} - (E_{eq,frag1} + E_{eq,frag2})$$

where *TS,frag1,2* represent individual fragments in their distorted transition state geometries; and *eq,frag1,2* represent individual fragments in their optimized, equilibrium ground-state geometries; the interaction energy is given by:

$$E_{int} = E_{TS} - (E_{TS,frag1} + E_{TS,frag2})$$

which accounts for the stabilizing interactions (e.g., electrostatic, orbital, dispersion) between the distorted fragments in the TS.

Thus, the total activation energy is given by:

$$\Delta E^\ddagger = E_{dist} + E_{int.}$$

Note that this single point activation energy and the activation energy differences $\Delta\Delta E^\ddagger$ between the major and minor TSs may be different from the Gibbs energy differences $\Delta\Delta G^\ddagger$ that is computed fully (including vibrational frequencies analysis) at SMD(DCM)-M06-2X/def2-TZVP//M06-2X/def2-SVP level of theory.

This analysis gives $\Delta\Delta E^\ddagger$ (NaOAc) as $\Delta\Delta E^\ddagger = 2.0$ kcal/mol in favor of the major product **TS_NaOAc_major** to minor product **TS_NaOAc_minor**, where the distortion

energy is 1.0 kcal/mol higher in **TS_NaOAc_major** whereas the interaction energy is more favorable, by 2.9 kcal/mol than in **TS_NaOAc_minor** (Table S6). Similarly, this analysis gives $\Delta\Delta E^\ddagger$ (DBU) as $\Delta\Delta E^\ddagger = 0.6$ kcal/mol in favor of the major product **TS_DBU_major** to minor product **TS_DBU_minor** (Table S6). In this case, **TS_DBU_major** benefits from lower distortion energy (by 14.5 kcal/mol) although it has a less favorable interaction energy (by 13.9 kcal/mol).

Table S6. Distortion-interaction analysis.

Transition State	ΔE^\ddagger	E_{dist}	E_{int}
TS_NaOAc_major	-4.4	46.4	-50.8
TS_NaOAc_minor	-2.5	45.4	-47.9
TS_DBU_major	-15.5	20.5	-36.0
TS_DBU_minor	-14.9	35.0	-49.9

8 Rotational Barrier of Product 4

DFT calculations were performed to obtain an estimate for the rotational barrier of product **4**. A relaxed potential energy surface (PES) scan along key dihedral angle was performed and the result is shown in Figure S6. We can see that the enantiomerization of product **4** proceeds via two stages: first, the dihedral rotation along one axial axis flips the aldehyde group from one side to the other (structure 1 to structure 4 in Figure S6). This has an estimated barrier of > 40 kcal/mol; then, dihedral angle rotation about the other axial axis flips the lactone group from one side (structure 4 through structure 6 to structure 7, Figure S6), giving a barrier of > 100 kcal/mol. This estimate looks *unreasonably high* and we performed a similar scan with the C=O group of the aldehyde pointing in the other direction, however, the relaxed PES scan produced *similarly high estimate* of the barrier. As such, we proceeded to locate the true transition state for the racemization.

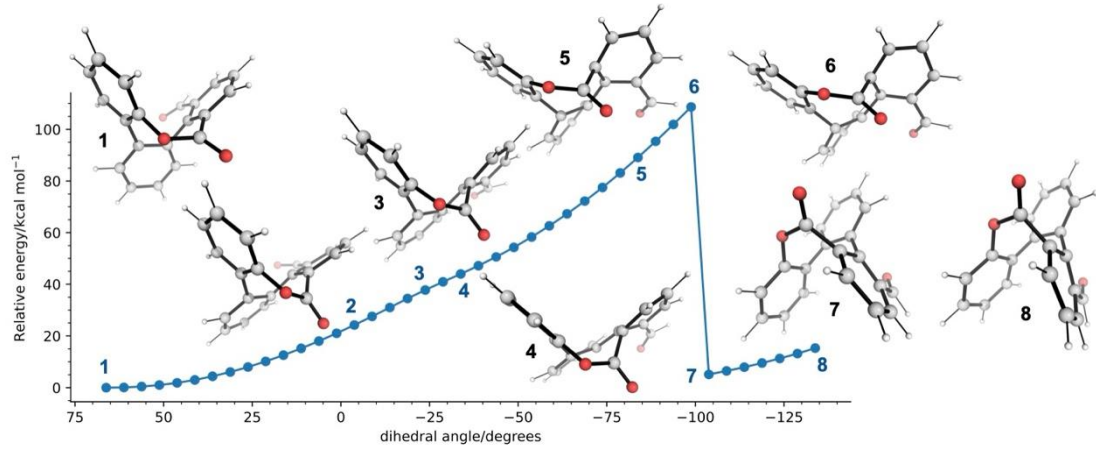


Figure S6. Relaxed potential energy surface (PES) scan to estimate the rotational barrier for product **4**.

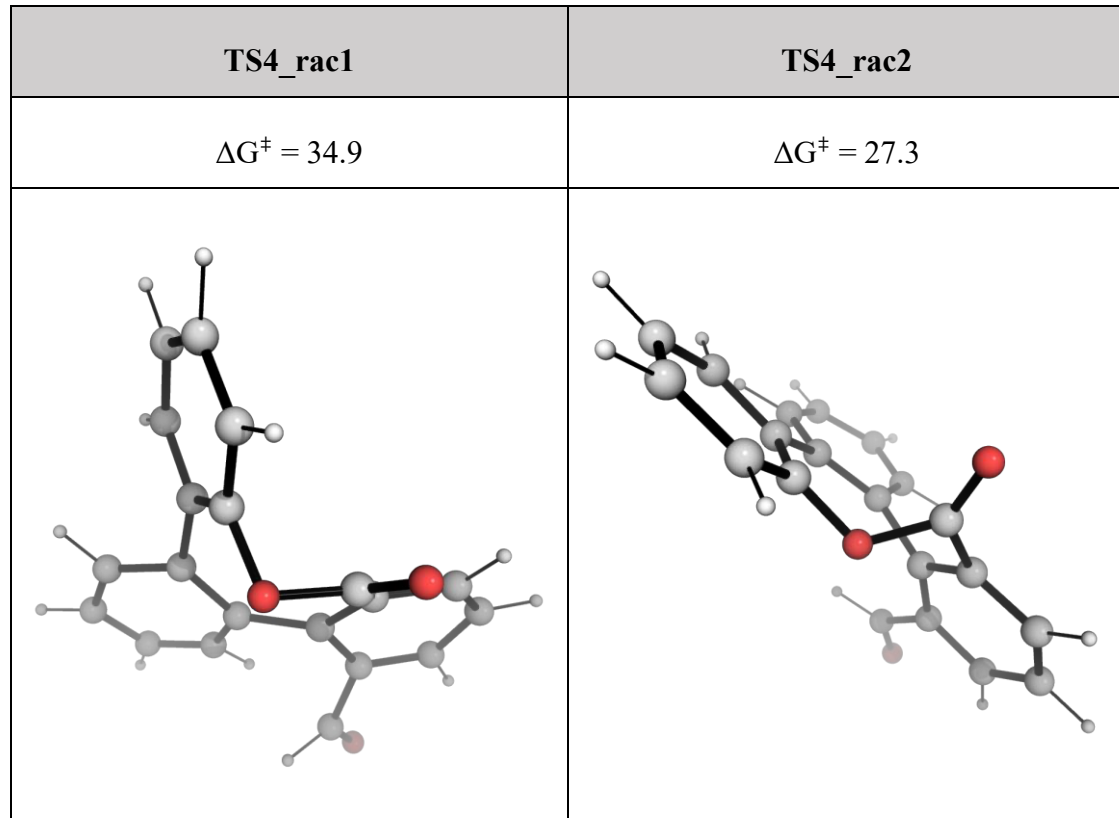


Figure S7. DFT-optimized structures for the transition states for the two-step racemization of product **4**.

We found that the racemization proceeds via a two-stage process, as indicated by the scan. We located the first step TS, which involves the flipping of aldehyde from one side of the axial axis to the other. This TS, **TS4_rac1**, shown in Figure S7, has a barrier

of 34.9 kcal/mol, relative to the energy of product **4**. This gives an intermediate, **INT4_rac**, at 26.8 kcal/mol, which subsequently undergoes a small-barrier TS, **TS4_rac2**, shown in Figure S7, at 27.3 kcal/mol (barrier of only 0.5 kcal/mol from **INT4_rac**, IRC-verified). that flips the lactone group from one side of the axis to the other. This gives the overall barrier for the racemization of product **4** as 34.9 kcal/mol. Thus, a word of caution should be noted that simple relaxed PES scan might overestimate the racemization barrier by a huge margin, especially for such inherently chiral compounds.

9 Simple transition state theory (TST) for rate estimation

The barrier difference $\Delta\Delta G^\ddagger$ between two transition states can be used to predict the kinetic preference for the major pathway over the minor pathway, using simple transition state theory as an estimate and without Boltzmann weighting of all the conformers.

The Eyring equation

$$k = \frac{k_B T}{h} e^{-\Delta G^\ddagger / RT}$$

gives the rate constant under simple transition state theory (TST) assumptions.

Under kinetic control, as we compare the barrier heights difference between competing transition states, the ratio of the rates between two pathways is given by:

$$\frac{k_A}{k_B} = \frac{e^{-\Delta G_A^\ddagger / RT}}{e^{-\Delta G_B^\ddagger / RT}} = e^{-\Delta\Delta G^\ddagger / RT}$$

where k_X is the rate constant of pathway X (X=A or B); ΔG_X^\ddagger is the activation barrier for pathway X; and $\Delta\Delta G^\ddagger$ is the difference in the barrier heights; and R is the gas constant, T the temperature. Note that the Eyring Equation pre-exponential factor cancels when comparing the ratio of the rate constants. Thus, using the calculated

$\Delta\Delta G_X^\ddagger$ value (difference of barrier heights between competing TSs) at the reaction temperature (e.g., 0°C = 273.15K), we are able to obtain the ratio of competing rates.

10 Optimised structures and absolute energies

Geometries of all optimised structures (in .xyz format with their associated gas-phase energy in Hartrees) are included in a separate folder named *DFT_optimized_structures*. All these data have been uploaded to zenodo.org <https://zenodo.org/records/15612293> (DOI: 10.5281/zenodo.15612293).

Absolute values (in Hartrees) for SCF energy, zero-point vibrational energy (ZPE), enthalpy and quasi-harmonic Gibbs free energy (at 0°C/273.15 K) for optimized structures are given below. Single point corrections in SMD DMF using M06-2X/def2-TZVP level of theory are also included.

Structure	E/au	ZPE/au	H/au	T.S/au	qh-G/au	SP
1a	-881.89591	0.278877	-881.60211	0.051849	-881.651955	-881.7244009
DBU	-461.536693	0.247404	-461.28021	0.03763	-461.317268	-461.453156
NaOAc	-390.49335	0.051237	-390.43605	0.030543	-390.46589	-390.4819475
INT1	-3192.799015	0.543674	-3192.2236	0.089312	-3192.3068	-3191.652202
INT1_c2	-3192.79802	0.543984	-3192.2224	0.089367	-3192.305459	-3191.648864
INT1_c3	-3192.796603	0.543915	-3192.221	0.090045	-3192.304411	-3191.646736
INT1_c4	-3192.792506	0.544394	-3192.2166	0.090629	-3192.299986	-3191.645169
INT1_c5	-3192.794624	0.543818	-3192.219	0.090921	-3192.302827	-3191.642422
INT1_c6	-3192.793959	0.544849	-3192.218	0.08779	-3192.299867	-3191.643527
INT1'	-3192.790276	0.543515	-3192.215	0.090347	-3192.298549	-3191.648992

INT1'_c2	-3192.790381	0.543731	-3192.2149	0.090078	-3192.29837	-3191.646493
INT1'_c3	-3192.786577	0.543666	-3192.2111	0.091527	-3192.295072	-3191.645966
INT1'_c4	-3192.791088	0.544347	-3192.2152	0.09049	-3192.298538	-3191.641866
TS_NaOAc_ma						
jor	-3583.337922	0.593395	-3582.7081	0.098198	-3582.800004	-3586.185692
TS_NaOAc_ma						
jor_c2	-3583.334982	0.592953	-3582.7053	0.100133	-3582.798144	-3586.181155
TS_NaOAc_mi						
nor	-3583.333478	0.592886	-3582.7039	0.100341	-3582.796763	-3586.182578
TS_NaOAc_mi						
nor_c2	-3583.329166	0.596053	-3582.6971	0.097596	-3582.78817	-3586.183047
TS_NaOAc_mi						
nor_c3	-3583.327754	0.595833	-3582.6959	0.097812	-3582.78701	-3586.180564
TS_DBU_minor	-3654.381653	0.789584	-3653.5516	0.109169	-3653.651743	-3657.430938
TS_DBU_minor						
_c2	-3654.366476	0.792011	-3653.5347	0.105284	-3653.632535	-3657.415838
TS_DBU_major	-3654.377826	0.789438	-3653.5479	0.109747	-3653.648169	-3657.431947
TS_DBU_major						
_c2	-3654.377469	0.789195	-3653.5478	0.109791	-3653.648069	-3657.430537
TS_DBU_major						
_c3	-3654.379842	0.790679	-3653.5492	0.106443	-3653.647716	-3657.432669
TS_DBU_major						
_c4	-3654.378459	0.790301	-3653.548	0.107626	-3653.647135	-3657.428854

4	-993.910886	0.267946	-993.62777	0.052393	-993.678304	-995.0367244
TS4_rac1	-993.858819	0.267911	-993.57687	0.049199	-993.625061	-994.9822921
INT4_rac	-993.869605	0.268313	-993.58638	0.051856	-993.636491	-994.9945477
TS4_rac2	-993.869024	0.268008	-993.58669	0.05012	-993.635486	-994.9942049

References

- (1) Zhou, Q. J.; Worm, K.; Dolle, R. E. 10-Hydroxy-10,9-boroxarophenanthrenes: Versatile Synthetic Intermediates to 3,4-Benzocoumarins and Triaryls. *J. Org. Chem.* **2004**, *69*, 5147-5149.
- (2) Kang, J.; Liu, J.; Chen, Z. Directing Group Controlled Regioselective C–H Borylation of 2-arylphenolic Compounds at Room Temperature. *Org. Chem. Front.* **2024**, *11*, 4249-4257

References for computational section

Full reference Gaussian 16:

Gaussian 16, Revision B.01, Frisch, M. J.; Trucks, G. W.; Schlegel, H. B.; Scuseria, G. E.; Robb, M. A.; Cheeseman, J. R.; Scalmani, G.; Barone, V.; Mennucci, B.; Petersson, G. A.; Nakatsuji, H.; Caricato, M.; Li, X.; Hratchian, H. P.; Izmaylov, A. F.; Bloino, J.; Zheng, G.; Sonnenberg, J. L.; Hada, M.; Ehara, M.; Toyota, K.; Fukuda, R.; Hasegawa, J.; Ishida, M.; Nakajima, T.; Honda, Y.; Kitao, O.; Nakai, H.; Vreven, T.; Montgomery Jr., J. A.; Peralta, J. E.; Ogliaro, F.; Bearpark, M.; Heyd, J. J.; Brothers, E.; Kudin, K. N.; Staroverov, V. N.; Kobayashi, R.; Normand, J.; Raghavachari, K.; Rendell, A.; Burant, J. C.; Iyengar, S. S.; Tomasi, J.; Cossi, M.; Rega, N.; Millam, J. M.; Klene, M.; Knox, J. E.; Cross, J. B.; Bakken, V.; Adamo, C.; Jaramillo, J.; Gomperts, R.; Stratmann, R. E.; Yazyev, O.; Austin, A. J.; Cammi, R.; Pomelli, C.; Ochterski, J. W.; Martin, R. L.; Morokuma, K.; Zakrzewski, V. G.; Voth, G. A.; Salvador, P.; Dannenberg, J. J.; Dapprich, S.; Daniels, A. D.; Farkas, Ö.; Foresman, J. B.; Ortiz, J. V.; Cioslowski, J.; Fox, D. J. Gaussian, Inc., Wallingford CT, 2016.

- (3) Frisch, M. J. ; Trucks, G. W. ; Schlegel, H. B. ; Scuseria, G. E. ; Robb, M. A. ; Cheeseman, J. R. ; Scalmani, G. ; Barone, V. ; Petersson, G. A. ; Nakatsuji, H. ; et al. Gaussian 16, Revision B.01. 2016.

- (4) Zhao, Y.; Truhlar, D. G. The M06 Suite of Density Functionals for Main Group Thermochemistry, Thermochemical Kinetics, Noncovalent Interactions, Excited States, and Transition Elements: Two New Functionals and Systematic Testing of Four M06-Class Functionals and 12 Other Function. *Theor. Chem. Acc.* **2008**, *120* (1), 215–241.
- (5) Weigend, F.; Ahlrichs, R. Balanced Basis Sets of Split Valence, Triple Zeta Valence and Quadruple Zeta Valence Quality for H to Rn: Design and Assessment of Accuracy. *Phys. Chem. Chem. Phys.* **2005**, *7* (18), 3297–3305.
- (6) Weigend, F. Accurate Coulomb-Fitting Basis Sets for H to Rn. *Phys. Chem. Chem. Phys.* **2006**, *8* (9), 1057–1065.
- (7) Zhang, X.; Paton, R. S. Stereoretention in Styrene Heterodimerisation Promoted by One-Electron Oxidants. *Chem. Sci.* **2020**, *11* (34), 9309–9324.
- (8) Yang, X.; Xie, Y.; Xu, J.; Ren, S.; Mondal, B.; Zhou, L.; Tian, W.; Zhang, X.; Hao, L.; Jin, Z.; et al. Carbene-Catalyzed Activation of Remote Nitrogen Atoms of (Benz)Imidazole-Derived Aldimines for Enantioselective Synthesis of Heterocycles. *Angew. Chem. Int. Ed.* **2021**, *60* (14), 7906–7912.
- (9) Li, B.; Hu, J.; Liao, M.; Xiong, Q.; Zhang, Y.; Chi, Y. R.; Zhang, X.; Wu, X. Catalyst Control over S(IV)-Stereogenicity via Carbene-Derived Sulfinyl Azolium Intermediates. *J. Am. Chem. Soc.* **2024**, *146*.
- (10) Song, R.; Liu, Y.; Majhi, P. K.; Ng, P. R.; Hao, L.; Xu, J.; Tian, W.; Zhang, L.; Liu, H.; Zhang, X.; et al. Enantioselective Modification of Sulfonamides and Sulfonamide-Containing Drugs: Via Carbene Organic Catalysis. *Org. Chem. Front.* **2021**, *8* (11), 2413–2419.
- (11) Lv, Y.; Luo, G.; Liu, Q.; Jin, Z.; Zhang, X.; Chi, Y. R. Catalytic Atroposelective Synthesis of Axially Chiral Benzonitriles via Chirality Control

- during Bond Dissociation and CN Group Formation. *Nat. Commun.* **2022**, *13* (1), 1–9.
- (12) Deng, R.; Wu, S.; Mou, C.; Liu, J.; Zheng, P.; Zhang, X.; Chi, Y. R. Carbene-Catalyzed Enantioselective Sulfonylation of Enone Aryl Aldehydes: A New Mode of Breslow Intermediate Oxidation. *J. Am. Chem. Soc.* **2022**, *144* (12), 5441–5449.
- (13) Lv, W. X.; Chen, H.; Zhang, X.; Ho, C. C.; Liu, Y.; Wu, S.; Wang, H.; Jin, Z.; Chi, Y. R. Programmable Selective Acylation of Saccharides Mediated by Carbene and Boronic Acid. *Chem* **2022**, *8* (5), 1518–1534.
- (14) Yang, X.; Wei, L.; Wu, Y.; Zhou, L.; Zhang, X.; Chi, Y. R. Atroposelective Access to 1,3-Oxazepine-Containing Bridged Biaryls via Carbene-Catalyzed Desymmetrization of Imines. *Angew. Chem. Int. Ed.* **2022**, *62* (1), e202211977.
- (15) Wei, L.; Li, J.; Zhao, Y.; Zhou, Q.; Wei, Z.; Chen, Y.; Zhang, X.; Yang, X. Chiral Phosphoric Acid Catalyzed Asymmetric Hydrolysis of Biaryl Oxazepines for the Synthesis of Axially Chiral Biaryl Amino Phenol Derivatives. *Angew. Chem. Int. Ed.* **2023**, *62* (39), e202306864.
- (16) Luo, Z.; Liao, M.; Li, W.; Zhao, S.; Tang, K.; Zheng, P.; Chi, Y. R.; Zhang, X.; Wu, X. Ionic Hydrogen Bond-Assisted Catalytic Construction of Nitrogen Stereogenic Center via Formal Desymmetrization of Remote Diols. *Angew. Chem. Int. Ed.* **2024**, e202404979.
- (17) Liu, D.; Tu, T.; Zhang, T.; Nie, G.; Liao, T.; Ren, S.-C.; Zhang, X.; Chi, Y. R. Photocatalytic Direct Para-Selective C–H Amination of Benzyl Alcohols: Selectivity Independent of Side Substituents. *Angew. Chem. Int. Ed.* **2024**, *63* (43), e202407293.
- (18) Marenich, A. V.; Cramer, C. J.; Truhlar, D. G. Universal Solvation Model Based on Solute Electron Density and on a Continuum Model of the Solvent

- Defined by the Bulk Dielectric Constant and Atomic Surface Tensions. *J. Phys. Chem. B* **2009**, *113* (18), 6378–6396.
- (19) Grimme, S. Supramolecular Binding Thermodynamics by Dispersion-Corrected Density Functional Theory. *Chem.: Eur. J.* **2012**, *18* (32), 9955–9964.
- (20) Luchini, G.; Alegre-Requena, J. V.; Funes-Ardoiz, I.; Paton, R. S. GoodVibes: Automated Thermochemistry for Heterogeneous Computational Chemistry Data. *F1000Research* **2020**, *9*, 291.
- (21) Bryantsev, V. S.; Diallo, M. S.; Goddard III, W. A.; Goddard, W. A. Calculation of Solvation Free Energies of Charged Solutes Using Mixed Cluster/Continuum Models. *J. Phys. Chem. B* **2008**, *112* (32), 9709–9719.
- (22) Boyle, B. T.; Levy, J. N.; de Lescure, L.; Paton, R. S.; McNally, A. Halogenation of the 3-Position of Pyridines through Zincke Imine Intermediates. *Science* **2022**, *378* (6621), 773–779.
- (23) Darù, A.; Hu, X.; Harvey, J. N. Iron-Catalyzed Reductive Coupling of Alkyl Iodides with Alkynes to Yield Cis-Olefins: Mechanistic Insights from Computation. *ACS Omega* **2020**, *5* (3), 1586–1594.
- (24) Contreras-García, J.; Johnson, E. R.; Keinan, S.; Chaudret, R.; Piquemal, J. P.; Beratan, D. N.; Yang, W. NCIPILOT: A Program for Plotting Noncovalent Interaction Regions. *J. Chem. Theory Comput.* **2011**, *7* (3), 625–632.
- (25) Schrödinger, L. *The PyMOL Molecular Graphics Development Component, Version 1.8*; 2015.
- (26) Grimme, S. Exploration of Chemical Compound, Conformer, and Reaction Space with Meta-Dynamics Simulations Based on Tight-Binding Quantum Chemical Calculations. *J. Chem. Theory Comput.* **2019**, *15* (5), 2847–2862.

- (27) Pracht, P.; Bohle, F.; Grimme, S. Automated Exploration of the Low-Energy Chemical Space with Fast Quantum Chemical Methods. *Phys. Chem. Chem. Phys.* **2020**, 22 (14), 7169–7192.
- (28) Bannwarth, C.; Ehlert, S.; Grimme, S. GFN2-XTB - An Accurate and Broadly Parametrized Self-Consistent Tight-Binding Quantum Chemical Method with Multipole Electrostatics and Density-Dependent Dispersion Contributions. *J. Chem. Theory Comput.* **2019**, 15 (3), 1652–1671.
- (29) Grimme, S.; Bannwarth, C.; Shushkov, P. A Robust and Accurate Tight-Binding Quantum Chemical Method for Structures, Vibrational Frequencies, and Noncovalent Interactions of Large Molecular Systems Parametrized for All Spd-Block Elements ($Z = 1\text{--}86$). *J. Chem. Theory Comput.* **2017**, 13 (5), 1989–2009.
- (30) Bannwarth, C.; Caldeweyher, E.; Ehlert, S.; Hansen, A.; Pracht, P.; Seibert, J.; Spicher, S.; Grimme, S. Extended Tight-Binding Quantum Chemistry Methods. *Wiley Interdiscip. Rev. Comput. Mol. Sci.* **2021**, 11 (2), e1493.
- (31) Ess, D. H.; Houk, K. N. Distortion/Interaction Energy Control of 1,3-Dipolar Cycloaddition Reactivity. *J. Am. Chem. Soc.* **2007**, 129, 10646–10647.
- (32) Bickelhaupt, F. M.; Houk, K. N. Analyzing Reaction Rates with the Distortion/Interaction-Activation Strain Model. *Angew. Chem. Int. Ed.* **2017**, 56, 10070–10086.